

Processing Pure Ti by High-Pressure Torsion in Wide Ranges of Pressures and Strain

KAVEH EDALATI, EIICHIRO MATSUBARA, and ZENJI HORITA

Pure Ti (99.4 pct) is processed by high-pressure torsion (HPT) at applied pressures in a wide range of 1.2 to 40 giga-pascals (GPa) for equivalent strain up to ~ 200 . X-ray diffraction (XRD) analysis clearly reveals that a pressure-induced phase transformation occurs from α phase to ω phase during HPT processing when the applied pressure is more than ~ 4 GPa and the straining facilitates this phase transformation. The hardness and the tensile strength increase, but the ductility decreases by the phase transformation. Hardness measurements demonstrate that all values obtained at each pressure fall on a single curve when they are plotted as a function of equivalent strain. The hardness increases with an increase in the equivalent strain at an early stage of straining and saturates to a constant level, where the hardness remains unchanged with further straining. It is shown that the saturation level as well as the onset of the saturation depends on the applied pressure.

DOI: 10.1007/s11661-009-9890-5

© The Minerals, Metals & Materials Society and ASM International 2009

I. INTRODUCTION

TO achieve ultra-fine-grained materials with grain sizes in the nanometer or submicrometer level, great attention has been allocated to the application of severe plastic deformation (SPD).^[1–6] Grain refinement using the SPD leads to an increase in the strength with reasonable ductility without addition of alloying elements. Pure Ti is a typical material in SPD-related research because of its biomedical application.^[7–9]

Different SPD methods have been used for processing of Ti. They are high-pressure torsion (HPT),^[10–12] equal-channel angular pressing (ECAP),^[13,14] ECAP followed by HPT,^[15,16] ECAP followed by cold rolling,^[17–19] accumulative roll bonding,^[20] multidirectional forging (MDF),^[21] and hydrostatic extrusion.^[22,23]

In the HPT method, a thin disc sample is placed between two anvils under a high pressure and intense shear strain is introduced by rotating the two anvils with respect to each other. To the best of the authors' knowledge, little is understood regarding the influence of the applied pressure on the mechanical properties and microstructures in HPT-processed Ti. The pressure for the HPT is normally in the range of several giga-pascals (GPa), but few experiments have been attempted with pressures higher than 8 GPa, except the application of 20 GPa for Fe.^[24]

Pure Ti may transform from an α phase with the hcp crystal structure to an ω phase with the simple

hexagonal structure.^[25–28] This phase transformation was observed using a diamond anvil cell at pressures greater than 2.9^[27] to 11 GPa.^[28] Errandonea *et al.*^[29] showed that such a pressure range for initiating the phase transformation is attributed to the presence of nonhydrostatic conditions arising from the difference in pressurizing media. The existence of a β phase with the bcc structure in Ti was also theoretically predicted at pressures higher than 36 GPa, but this transformation has never been observed experimentally.^[30,31] A survey of the literature concludes that, in spite of the numerous studies concerning the effect of pressure on the phase transformations in pure Ti, there are limited works on the role of strain for the pressure-induced phase transformations in Ti.^[32,33] Kilmametov *et al.*^[32] reported that the formation of an ω phase occurred in Ti even under a pressure of 3 GPa when HPT was used. Furthermore, it was reported that the fraction of ω phase increases with increasing pressure from 3 to 6 GPa and with increasing shear strain. All these results suggest the importance of not only pressure but also strain for the phase transformation in Ti.

In the present investigation, commercial pure Ti is processed by HPT to examine the evolution of mechanical properties and microstructural features including phase transformation. Both applied pressure and imposed strain are varied over wide ranges such that the pressure is raised to 40 GPa, which is the largest pressure attempted in the HPT studies and the equivalent strain of up to ~ 200 is produced by increasing the number of revolutions in HPT.

II. EXPERIMENTAL MATERIALS AND PROCEDURES

A rod of commercial pure Ti (99.4 pct) with 10-mm diameter and 70-mm length was used in this study.

KAVEH EDALATI, Graduate Student, and ZENJI HORITA, Professor, are with the Department of Materials Science and Engineering, Faculty of Engineering, Kyushu University, Fukuoka 819-0395, Japan. Contact e-mail: kaveh.edalati@zaiko6.zaiko.kyushu-u.ac.jp EIICHIRO MATSUBARA, Professor, is with the Department of Materials Science and Engineering, Faculty of Engineering, Kyoto University, Kyoto 606-8501, Japan.

Manuscript submitted October 4, 2008.

Article published online June 30, 2009

The Ti rod had impurities of H0.013, O0.20, N0.05, and Fe0.25 (wt pct). The rod was annealed for 1 hour at 1073 K under an argon atmosphere and sliced to discs with thicknesses of 0.85 mm using a wire-cutting electric discharge machine. In addition, disc samples with 4-mm diameter and 0.85-mm thickness were prepared for pressures higher than 6 GPa.

The HPT was carried out on the annealed discs. Two sets of upper and lower anvils with a circular flat-bottom hole at the center were used to process the disc samples where the hole depths were 0.25 mm and hole diameters were 4 and 10 mm, respectively. The disc samples with 10-mm diameter were processed to either 1/2, 1, 2, 4, or 10 revolutions with rotation speeds of 0.2 and 0.5 rpm under a selected load in the range of 9.6 to 48 tons. These loads are equivalent to the pressures in the range of 1.2 to 6 GPa. The disc samples with 4-mm diameter were processed with a rotation speed of 0.2 rpm under a selected load in the range of 17.5 to 50 tons for 5 revolutions, and these loads are equivalent to the pressures in the range of 14 to 40 GPa. It should be noted that the pressure was calculated by dividing the applied load by the area of the central hole on the anvil. Nevertheless, the pressure was not rigorously evaluated in this study because of the difficulty in direct measurement under very restricted conditions so that it should be taken as the nominal pressure in this study. A thermocouple located at the center of the upper anvil and at the position 10 mm away from the surface was used to check the temperature rise during HPT.

The disc samples with 10-mm diameter after HPT were evaluated in terms of Vickers microhardness, tensile properties, microstructures, and X-ray diffraction (XRD). First of all, after processing by HPT, disc samples were polished to a mirrorlike surface and the Vickers microhardness was measured with an applied load of 200 g for 15 seconds along the radii from the center to edge at eight different radial directions with 0.5-mm increments, as drawn by dotted lines in Figure 1 for 10-mm discs. For the 4-mm discs, the hardness measurements were undertaken at positions 1.5 mm

away from the center in eight radial directions after polishing to a mirrorlike surface.

Second, miniature tensile specimens having 1-mm gage length, 1-mm width, and 0.5-mm thickness were cut from the 10-mm discs at the position 2 mm away from the center, as illustrated in Figure 1. Each tensile specimen was mounted horizontally on grips and pulled to failure using a tensile testing machine with an initial strain rate of $3.3 \times 10^{-3} \text{ s}^{-1}$. The stress-strain curve was plotted for each specimen and the ultimate tensile strength (UTS) and elongation to failure were measured from the curves. It should be noted that the dimensions of the present tensile specimens are fairly small, and therefore, care is required when compared with other dimensions of tensile specimens, as pointed out by Zhao *et al.*^[34]

Third, for transmission electron microscopy (TEM), discs with 3-mm diameter were punched out from the 10-mm HPT discs at 3.5 mm away from the center, as illustrated in Figure 1. The 3-mm discs were ground mechanically to a thickness of 0.15 mm and further thinned for electron transparency with a twin-jet electrochemical polisher using a solution of 4 pct HClO_4 , 25 pct $\text{C}_3\text{H}_5(\text{CH}_2)_2\text{CH}_2\text{OH}$, and 69 pct CH_3OH at 243 K under an applied voltage of 10 V. A Hitachi H-8100 transmission electron microscope (Hitachi Naka-shi, Ibaraki, Japan) was operated at 200 kV for microstructural observation. Selected area electron diffraction (SAED) patterns were taken from a region with 6.3- μm diameter to complement the TEM observation.

Fourth, disc samples processed under different pressures including an annealed disc before HPT were polished to a mirrorlike surface, and the structural analysis with XRD was performed using the $\text{Co } K_\alpha$ radiation ($\lambda = 1.79 \text{ \AA}$) in a scanning step of 0.01 deg and a scanning speed of 2 deg/min.

III. RESULTS

Microhardness measurements have confirmed that the hardness increases with the distance from the disc center for all numbers of revolutions and the hardness level is higher for larger numbers of revolutions, as in other reports.^[4,35–37] All hardness values are then plotted against the equivalent strain in Figure 2, as attempted earlier on Al,^[38,39] Cu,^[35,39] and Fe.^[36] Here, the equivalent strain was calculated through the following equation:^[36]

$$\varepsilon = (1 - s) \int_0^\theta \frac{r}{\sqrt{3}t(\theta)} d\theta \quad [1]$$

where s is the fraction of slippage, r is the distance from the disc center, θ is the rotation angle in radians, and t is the thickness of the disc. This equation is a modified form of that presented earlier,^[39] and it takes into account the effects of the slippage between the sample and anvil and of the thickness reduction during HPT operation. The applicability and importance of this equation were given in a recent article.^[36] In this study, the values of s were measured as 0.23, 0.19, and 0.03 for

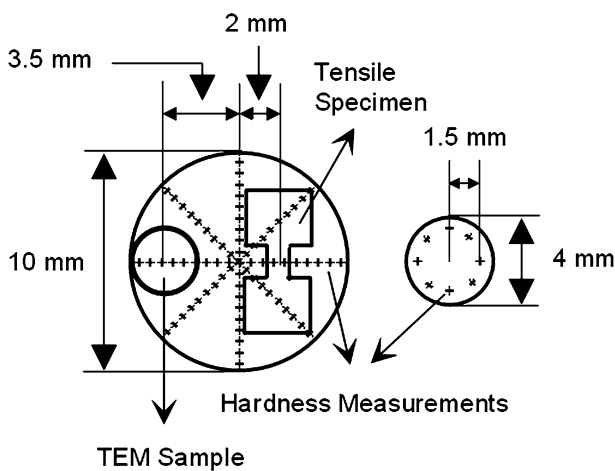


Fig. 1—Schematic illustration of HPT discs and procedures for microhardness measurements and locations for TEM disc and tensile testing specimen.

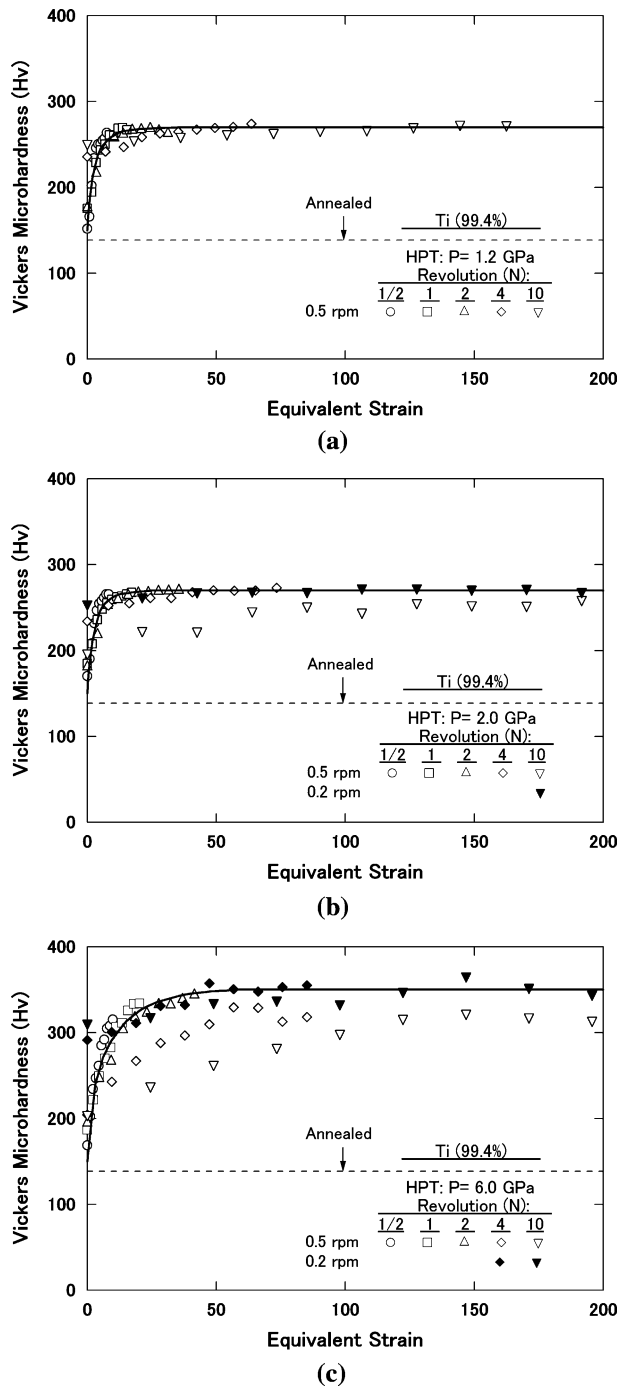


Fig. 2—Vickers microhardness plotted against equivalent strain for samples processed under pressures of (a) 1.2 GPa, (b) 2 GPa, and (c) 6 GPa and various revolutions.

the applied pressures of 1.2, 2, and 6 GPa, respectively, following the manner described earlier.^[40] Because t was changed with θ , the functional forms of $t(\theta)$ were determined for the three different pressures, as described in the Appendix.

Figure 2 shows that all points tend to fall on a single curve for each pressure, but deviation occurs in Figures 2(b) and (c), which corresponds to the samples processed for 4 and 10 revolutions with a rotation speed

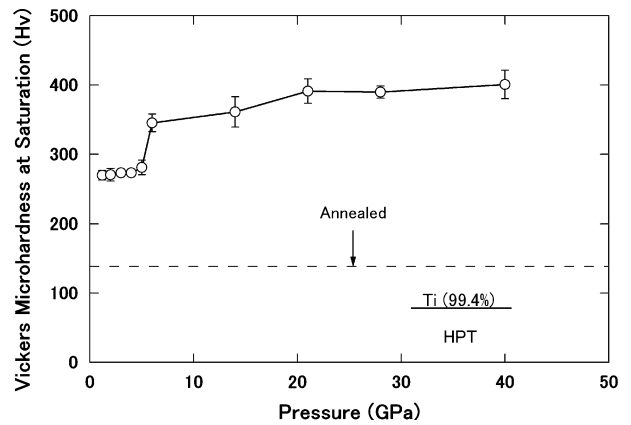


Fig. 3—Plots of Vickers microhardness at saturation with respect to pressure.

of 0.5 rpm. This deviation can be attributed to heat generation in these samples. More details for the temperature rise are discussed later. The microhardness increases with increasing equivalent strain at early stages of straining but saturates to steady levels where the hardness remains unchanged with further straining. The microhardness at the saturated level is the same for the applied pressures of 1.2 and 2 GPa but is higher for the pressure of 6 GPa. The critical equivalent strains at the onset of the saturation are ~ 20 , ~ 10 , and ~ 50 for the applied pressures of 1.2, 2, and 6 GPa, respectively.

The microhardness at the saturation is plotted in Figure 3 as a function of the applied pressure for an extended range to 40 GPa covered in this study. The saturation microhardness is almost constant until the abrupt increase occurs at a pressure of 4 GPa, and with a further increase in the pressure, the saturation hardness gradually increases over a range up to 40 GPa.

The variations of the UTS and the total elongation to failure are plotted against the applied pressure in Figures 4(a) and (b), respectively, for samples after 10 revolutions. The tensile specimens were prepared 2 mm away from the disc center, as shown in Figure 1, so that the tensile properties reflect the saturated levels. The UTS is almost constant for the pressures up to 4 GPa followed by an increase in the tensile strength at 5 and 6 GPa. This trend is very similar to the hardness variation shown in Figure 3. The variation of the total elongation to failure is opposite to the UTS: the elongation to failure remains almost constant for the applied pressures up to 4 GPa but decreases with further increasing the pressure and reaches zero at the pressure of 6 GPa.

The TEM microstructures were shown in Figure 5 for samples after 10 revolutions under three different pressures: (a) and (b) 1.2 GPa, (c) and (d) 2 GPa, and (e) and (f) 6 GPa. A bright-field image (left) and a dark-field image (right) including the corresponding SAED pattern (center) were shown for each pressure. Note that the dark-field images were taken with the diffracted beams indicated by arrows in the SAED patterns. It should be noted that all TEM samples were prepared from the positions away from the center, as shown in

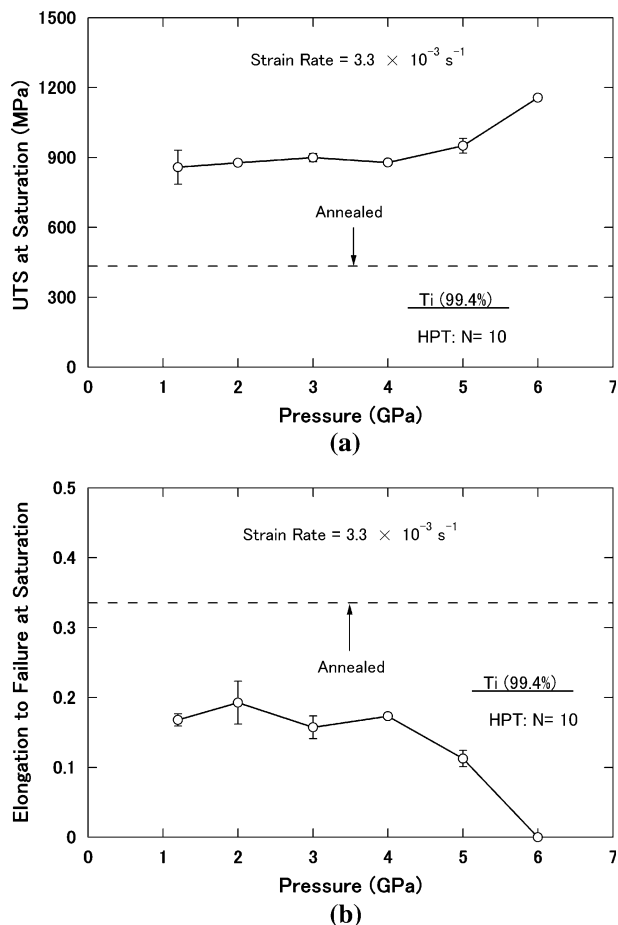


Fig. 4—Plots of (a) UTS at saturation and (b) elongation to failure at saturation with respect to pressure.

Figure 1, and they correspond to the saturated levels. It is apparent from Figures 5(a) through (f) that the microstructure consists of small grains with submicrometer sizes and many of the grains are surrounded by curved or ill-defined grain boundaries. Many strained contrasts are visible in the small grains and they can be mostly associated with dislocations. The SAED analysis exhibits well-defined ring patterns, indicating that the grain boundaries are in high angles of misorientation. These microstructural features are common at the three applied pressures and are similar to earlier observations of not only Ti and Ti alloys^[10–16] but also other metallic materials.^[35,36] However, measurements from several dark-field images reveal that the grain size for the pressure of 6 GPa is appreciably finer than that for the pressure of 1.2 GPa: ~200 nm for 1.2 GPa and ~150 nm for 6 GPa. It is considered that this is due to the formation of the ω phase, which acted as an inhibitor for the motions of dislocations and grain boundaries.

Figure 6 shows XRD profiles for samples processed at a pressure in the range of 1.2 to 40 GPa, including the annealed sample. The peak for an ω phase clearly appears above the pressure of 4 GPa, and this formation is consistent with earlier studies reporting the transformation from α phase to ω phase at a pressure of 2.9 to

11 GPa.^[27–29] It is also found from Figure 6 that the fraction of the ω phase increases with the applied pressure, because the relative peak heights of the ω phase to the α phase increase with the applied pressure above 4 GPa.

The XRD profiles for different numbers of revolutions at an applied pressure of 6 GPa are shown in Figure 7. No visible peak is detected for the ω phase after application of the pressure but without rotation. However, a peak for the ω phase clearly appears after rotation by 1/2 and the peak height increases with further revolution. This indicates that no phase transformation occurs by mere application of the pressure and the straining is effective for the phase transformation. A comparison of the peak heights between the α phase and the ω phase in Figure 7 reveals that there should be an intimate crystallographic correlation between the formation of the ω phase and disappearance of the α phase. This is because the relative intensity of the $(1010)_{\omega}$ peak to the $(0002)_{\alpha}$ peak is increased with straining despite the fact that the $(1011)_{\alpha}$ peak remains the same height. It is suggested that the formation of the ω phase may occur by rearrangement of atoms in the $(0002)_{\alpha}$ plane in consistency with earlier reports.^[26,41]

Figure 8 shows XRD profiles for the discs subjected to HPT at a pressure of 2 GPa. No ω -phase peaks are present because the applied pressure is less than 4 GPa. Not only the peak broadening but also the change in peak height occurs significantly by compression and subsequent rotation through HPT; in particular, the $(0002)_{\alpha}$ peak appears strongly. The appearance of the $(0002)_{\alpha}$ peak indicates that a texture develops at the early stages of torsional straining such that the basal planes of the α phase with the hcp crystal structure tend to be parallel to the disc surface. This is reasonable because the basal planes are oriented to be parallel to the shear plane by the compression and subsequent rotation through HPT. More importantly, the absence of the ω -phase peaks indicates that the pressure more than a critical value is required for the phase transformation to occur. Straining is then used to assist the procession of the phase transformation but is not a factor in initiating transformation.

IV. DISCUSSION

This study has clearly demonstrated that the phase transformation occurs from α phase to ω phase during HPT processing. Applied pressure is an important factor in initiating the phase transformation, and it is necessary to apply a pressure that is greater than the critical value, which was about 4 GPa in this study. Straining is also important, but it has a role in facilitating the phase transformation not in initiating it. It is important to note that the fraction of the ω phase was confirmed to remain constant even after maintaining it for 400 days at ambient pressure following processing by HPT at 6 GPa for 10 revolutions. This indicates that the straining is also important in inhibiting reverse transformation.

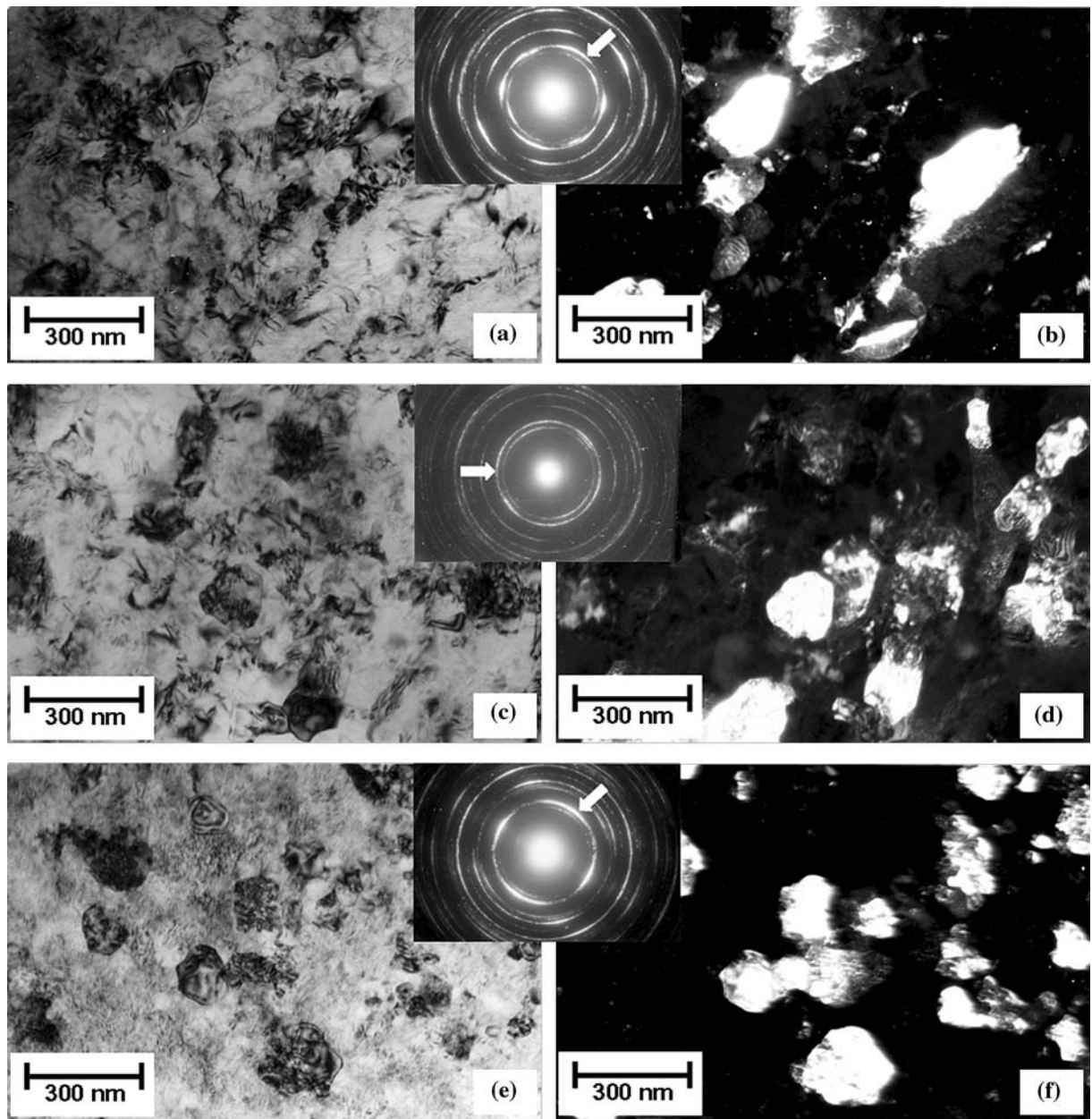


Fig. 5—TEM bright- and dark-field images and SAED patterns for samples processed under pressures of (a) and (b) 1.2 GPa, (c) and (d) 2 GPa, and (e) and (f) 6 GPa after 10 revolutions.

Close observation of Figures 2(b) and (c) shows that, if the rotation speed is high (as 0.5 rpm) and the revolution numbers are large (as 10), the hardness level is lowered. It is considered that this is due to the heat generation and subsequent temperature rise during HPT processing. The heat generation should be more intense as the imposed strain is larger, the strain rate is higher, and the applied pressure is higher. Thus, to check the effect of temperature rise on the hardness level, two additional measurements were carried out in this study.

First, the temperature was recorded during HPT with an anvil having a hole for a thermocouple, which was terminated at a position 10 mm from the disc sample.

The measurements showed that the temperature increases with increasing the number of revolutions, the rotation speed, and the loading pressure. In fact, this tendency is consistent with the downward deviation of data points shown in Figures 2(b) and (c). Although the temperature rise was small, reaching $\sim 45^\circ\text{C}$ at the conditions for $N = 10$ and $P = 2$ GPa with a rotation speed of 0.5 rpm, the true temperature on the sample should be higher than the measured one due to the position of the thermocouple, which is 10 mm away from the small sample in the massive anvils.

Second, differential scanning calorimetry experiments confirmed that reverse transformation from the ω phase

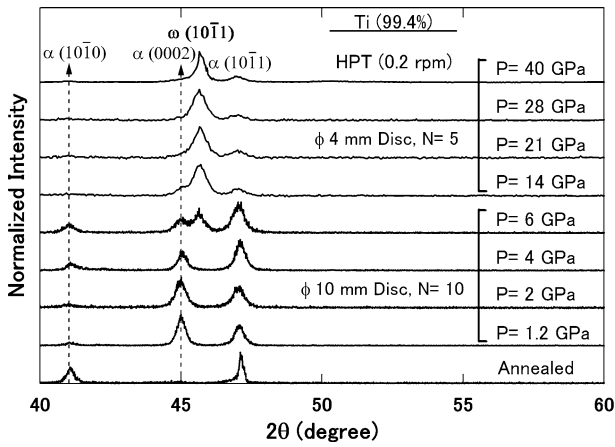


Fig. 6—XRD profiles of Ti at steady state under pressures in the range of $P = 1.2$ to 40 GPa including annealed sample.

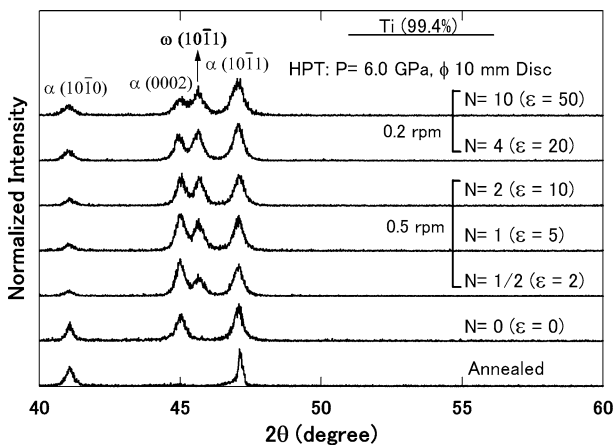


Fig. 7—XRD profiles of Ti processed at 6 GPa for revolutions of $N = 0$ to 10 including annealed sample.

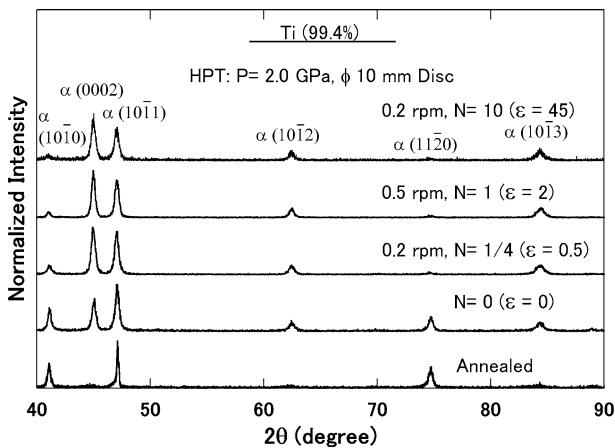


Fig. 8—XRD profiles of Ti processed at 2 GPa and after various revolutions including annealed sample.

to the α phase occurs at 150 °C. The temperature rise might have reached 150 °C, which can be sufficient to cause reverse transformation from ω phase to α phase.

It is reasonable that lowering the hardness is more pronounced, as shown in Figure 2(c), for $N = 10$ at $P = 6$ GPa.

Further examination of Figures 2(a) and (b) shows that the hardness increases more rapidly with increasing equivalent strain as the pressure increases from 1.2 to 2 GPa and the critical equivalent strain for the saturation decreases from ~ 20 to ~ 10 . However, the saturation level is independent of the applied pressure for up to 4 GPa, as shown in Figure 3. This trend is consistent with the behavior of pure Cu and Fe^[42] and can be accounted for by the idea that high pressures suppress atomic diffusion and dislocation recovery^[43,44] to increase dislocation density and thus to saturate more readily to the constant level. For pressures higher than 4 GPa, the hardness gradually increases to the level in saturation and the critical equivalent strain is increased to ~ 50 at the pressure of 6 GPa, as in Figure 2(c). This should be due to a strain-assisted ω -phase formation, and thus, the amount of the ω phase is increased to the equilibrium fraction determined by the applied pressure. The hardness at the saturation gradually increases with the pressure, as shown in Figure 3, because of an increase in the equilibrium fraction of the ω phase, which is known to be harder than the α phase.^[26] It should be noted that, because the grain size becomes finer, as commented in Figure 5, this grain refinement can be another cause for increasing the hardness at the pressures above 4 GPa.

There may be an additional factor involved in discussing the effect on the microstructural development and subsequent mechanical properties; this factor is the strain rate, which is expressed as a function of the distance from the disc center, as readily derived from Eq. [1]. As shown in Figure 2, all hardness values are well on a single curve for a given applied pressure despite the fact that the strain rate is different. This suggests that the effect of strain rate on the mechanical properties is of little significance within the magnitude (0 to 0.2 s⁻¹) covered in this study when compared with the effect of strain.

Based on the results obtained in this study, the hardness behavior of Ti with straining by HPT is delineated in Figure 9 for different applied pressures. For the pressure below 4 GPa, where no phase transformation occurs, the hardness increases with straining and saturates to a constant level, which was 265 Hv in this study. The critical strain to saturation becomes smaller as the pressure increases. When the transformation occurs as the pressure exceeds the critical value, the hardness gradually increases with straining. The transformation can be assisted by straining and the gradual increase in hardness continues until it reaches a constant level. The hardness increase can be due to the increase in the fraction of ω phase, which is harder than the α phase; in addition, the grain refinement by intense straining may contribute to the hardness increase. For the applied pressure well above the critical pressure, the hardness behavior is given by the broken lines. The ω phase dominates the entire sample from an early stage of straining. This hardness behavior with strain can be very similar to the case where the pressure below 4 GPa is

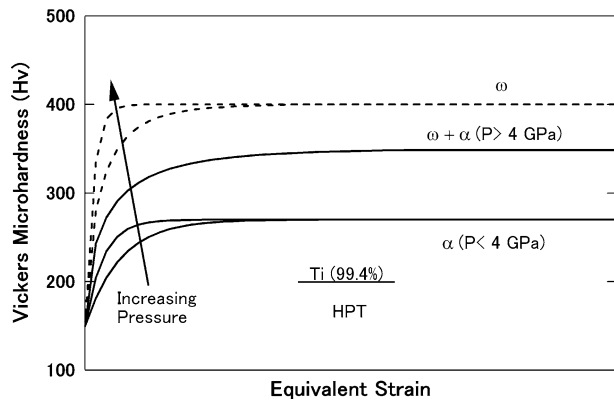


Fig. 9—Illustration of hardness behavior of Ti with straining based on HPT experiments.

applied, except that the former hardness level is higher than the latter.

Finally, we should mention that no peak related to a β phase was detected in the XRD profiles obtained at higher applied pressures even after intense straining. Although the formation of the β phase with the bcc structure in Ti was theoretically predicted at pressures higher than 36 GPa, this transformation was not observed in this study as in earlier reports.^[30,31]

V. CONCLUSIONS

1. The phase transformation occurs from α phase to ω phase during HPT processing of commercial pure Ti (99.4 pct). Applied pressure is an important factor in initiating the phase transformation, and straining has a role facilitating the α phase to ω phase transformation.
2. For the phase transformation to occur, it is necessary to apply a pressure greater than ~ 4 GPa. The strain rate has little significance on the α to ω transformation. The reverse transformation from the ω phase to α phase occurs when the temperature increases more than ~ 150 °C.
3. The α to ω transformation leads to an increase in the hardness and UTS but to a decrease in the ductility in the pressure range greater than 4 GPa.
4. When all hardness values at each applied pressure are plotted as a function of equivalent strain, they lie well on a single curve. The hardness increases with an increase in the equivalent strain and saturates into a steady-state level. The deviation from the curve is due to heat generation and subsequent temperature rise during HPT processing.
5. The critical equivalent strain for entering the saturation level decreases with increasing the applied pressure but below the pressure for the phase transformation ($< \sim 4$ GPa), and this is consistent with other pure metals. However, the critical equivalent strain increases for the pressures ($> \sim 4$ GPa) where the phase transformation occurs.
6. The XRD analysis confirmed that the phase transformation from α phase to ω phase occurs with an

atomic rearrangement of the $(0002)_\alpha$ plane and the fraction of ω phase increases with straining and pressure.

ACKNOWLEDGMENTS

One of the authors (KE) thanks the Islamic Development Bank for a scholarship. This work was supported in part by the Light Metals Educational Foundation of Japan; in part by a Grant-in-Aid for Scientific Research from the Ministry of Education, Culture, Sports, Science and Technology, Japan, in Priority Areas “Giant Straining Process for Advanced Materials Containing Ultra-High Density Lattice Defects”; and in part by Kyushu University Interdisciplinary Programs in Education and Projects in Research Development (P&P).

APPENDIX

Figure A1 plots the thickness as a function of θ measured after HPT at three different pressures, 1.2, 2, and 6 GPa. The measurements were made using a micrometer with an accuracy of ± 0.002 mm, and it was found that the discs after HPT were acceptably flat with the maximum difference of 0.02 mm along the radius. The thickness decreases rapidly within the first few revolutions and gradually thereafter. The variation with respect to rotation angle can be best expressed with the forms given in the figures. For each equation, the value of the first term, 0.5, arises because the thickness never decreases below 0.5 mm due to the hole depth of 0.25 mm for each of the upper and lower anvils. The second term represents the reduction in thickness with rotation angle. With such fitting functions, the thickness is 0.85 mm when the rotation angle is zero, which represents the initial thickness of disc, and the thickness reaches 0.5 mm when the rotation angle is infinitely large.

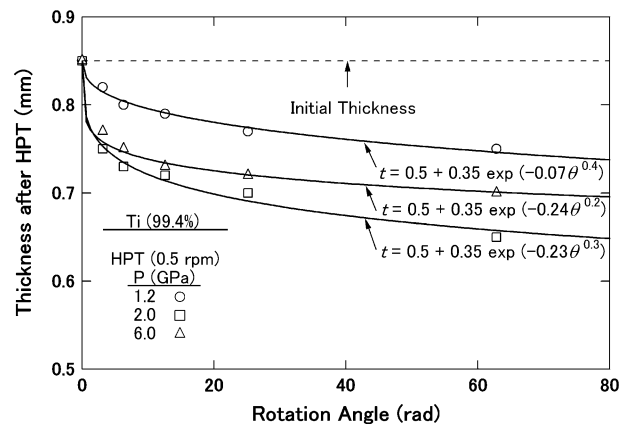


Fig. A1—Thickness after HPT plotted against rotation angle for samples processed at different pressures. Lines with equations represent fitting.

REFERENCES

- R.Z. Valiev, R.K. Islamgaliev, and I.V. Alexandrov: *Prog. Mater. Sci.*, 2000, vol. 45, pp. 103–89.
- Y. Iwahashi, Z. Horita, M. Nemoto, and T.G. Langdon: *Acta Mater.*, 1997, vol. 45, pp. 4733–41.
- Y. Iwahashi, Z. Horita, M. Nemoto, and T.G. Langdon: *Acta Mater.*, 1998, vol. 46, pp. 3317–31.
- G. Sakai, Z. Horita, and T.G. Langdon: *Mater. Sci. Eng. A*, 2005, vol. 393, pp. 344–51.
- N.A. Smirnova, V.I. Levit, V.I. Pilyugin, R.I. Kuznetsov, L.S. Davydova, and V.A. Sazonova: *Fiz. Met. Metalloved.*, 1986, vol. 68, pp. 1170–77.
- A.P. Zhilyaev, G.V. Nurislamova, B.K. Kim, M.D. Baro, J.A. Szpunar, and T.G. Langdon: *Acta Mater.*, 2003, vol. 51, pp. 753–65.
- V.V. Stolyarov, V.V. Latysh, R.Z. Valiev, Y.T. Zhu, and T. Lowe: *Proc. NATO ARW on Investigation and Application of Severe Plastic Deformation*, T. Lowe and R. Valiev, eds., Moscow, Dordrecht, Russia, 1999, p. 367.
- V.S. Zhernakov, V.V. Latysh, V.V. Stolyarov, A.I. Zharikov, and R.Z. Valiev: *Scripta Mater.*, 2001, vol. 44, pp. 1771–74.
- R.Z. Valiev, I.P. Semenova, E. Jakushina, V.V. Latysh, H. Rack, T.C. Lowe, J. Petruzelka, L. Dluhos, D. Hrusak, and J. Sochova: *Mater. Sci. Forum*, 2008, vols. 584–586, pp. 49–54.
- S. Faghihi, A.P. Zhilyaev, J.A. Szpunar, F. Azari, H. Vali, and M. Tabrizian: *Adv. Mater.*, 2007, vol. 19, pp. 1069–73.
- A.A. Propov, Y.U.I. Pyshmintsev, S.L. Demakov, A.G. Illarionov, T.C. Lowe, A.V. Segeyeva, and R.Z. Valiev: *Scripta Mater.*, 1997, vol. 37, pp. 1089–94.
- A.V. Sergueeva, V.V. Stolyarov, R.V. Valiev, and A.K. Mukhrjee: *Scripta Mater.*, 2001, vol. 45, pp. 747–52.
- D.H. Shin, I. Kim, J. Kim, Y.S. Kim, and S.L. Semiatin: *Acta Mater.*, 2003, vol. 51, pp. 983–96.
- A.Y. Vinogradov, V.V. Stolyarov, S. Hashimoto, and R.Z. Valiev: *Mater. Sci. Eng. A*, 2001, vol. 318, pp. 163–73.
- V.V. Stolyarov, Y.T. Zhu, T.C. Lowe, R.K. Islamgaliev, and R.Z. Valiev: *Nanostruct. Mater.*, 1999, vol. 11, pp. 947–54.
- R.Z. Valiev, A.V. Sergueeva, and A.K. Mukherjee: *Scripta Mater.*, 2003, vol. 49, pp. 669–74.
- V.V. Stolyarov, Y.T. Zhu, I.V. Alexandrov, T.C. Lowe, and R.Z. Valiev: *Mater. Sci. Eng. A*, 2003, vol. 343, pp. 43–50.
- V.V. Stolyarov, Y.T. Zhu, G.I. Raab, A.I. Zharikov, and R.Z. Valiev: *Mater. Sci. Eng. A*, 2004, vol. 385, pp. 309–13.
- Y.T. Zhu, J.Y. Huang, J. Gubicza, T. Ungar, Y.M. Wang, E. Ma, and R.Z. Valiev: *J. Mater. Res.*, 2003, vol. 18 (8), pp. 1908–17.
- D. Terada, S. Inoue, and N. Tsuji: *J. Mater. Sci.*, 2007, vol. 42, pp. 1673–81.
- G.A. Salishchev, R.M. Galeev, S.P. Malysheva, and M.M. Myshleav: *Nanostruct. Mater.*, 1999, vol. 11 (3), pp. 407–14.
- K.J. Kurzydowski, H. Garbacz, and M. Richert: *Rev. Adv. Mater. Sci.*, 2004, vol. 8, pp. 129–33.
- J. Dutkiewicz, J. Kusnierz, W. Maziarz, M. Lejkowska, H. Garbacz, M. Lewandowska, A.V. Dobromyslov, and K.J. Kurzydowski: *Phys. Status Solidi*, 2005, vol. 202 (12), pp. 2309–20.
- V.N. Varyukhin and B.M. Efron: *Proc. Nanostructured Materials by High-Pressure Severe Plastic Deformation*, Y.T. Zhu and V. Varyukhin, eds., Springer, Dordrecht, the Netherlands, 2006, vol. 212, pp. 13–20.
- A.R. Kutsar: *Fiz. Met. Metalloved.*, 1975, vol. 40, pp. 786–93.
- S.K. Sikka, Y.K. Vohra, and R. Chidambaram: *Prog. Mater. Sci.*, 1982, vol. 27, pp. 245–310.
- Y. K. Vohra, S.K. Sikka, S.N. Vaidya, and R. Chidambaram: *J. Phys. Chem. Solids*, 1977, vol. 38 (11), pp. 1293–96.
- C.W. Greeff, D.R. Trinkle, and R.C. Albert: *J. Appl. Phys.*, 2001, vol. 90 (5), pp. 2221–26.
- D. Errandonea, Y. Meng, M. Somayazulu, and D. Haussermann: *Physica B*, 2005, vol. 355, pp. 116–25.
- Y.K. Vohra and P.T. Spencer: *Phys. Rev. Lett.*, 2001, vol. 86 (14), pp. 3068–71.
- Y. Akahama, H. Kawamura, and T.L. Bihan: *Phys. Rev. Lett.*, 2001, vol. 87, p. 275503.
- A.R. Kilmametov, A.V. Khristoforova, G. Wilde, and R.Z. Valiev: *Z. Kristallogr.*, 2007, vol. 2007 (26), pp. 339–44.
- Y. Todaka, J. Sasaki, T. Moto, and M. Umamoto: *Scripta Mater.*, 2008, vol. 59, pp. 615–18.
- Y.H. Zhao, Y.Z. Guo, Q. Wei, A.M. Dangelewicz, C. Xu, Y.T. Zhu, T.G. Langdon, Y.Z. Zhou, and E.J. Lavernia: *Scripta Mater.*, 2008, vol. 59, pp. 627–30.
- Y. Harai, Y. Ito, and Z. Horita: *Scripta Mater.*, 2008, vol. 58, pp. 469–72.
- Y. Ito, Y. Harai, T. Fujioka, K. Edalati, and Z. Horita: *Mater. Sci. Forum*, 2008, vols. 584–586, pp. 191–96.
- K. Edalati, T. Fujioka, and Z. Horita: *Mater. Sci. Eng. A*, 2008, vol. 497, pp. 168–73.
- K. Edalati, T. Fujioka, and Z. Horita: *Mater. Trans.*, 2009, vol. 50, pp. 44–50.
- A. Vorhauer and R. Pippan: *Scripta Mater.*, 2004, vol. 51, pp. 921–25.
- K. Edalati, Z. Horita, and T.G. Landgon: *Scripta Mater.*, 2009, vol. 60, pp. 9–12.
- J.M. Silcock: *Acta Metall.*, 1958, vol. 6, pp. 481–93.
- K. Edalati, T. Fujioka, and Z. Horita: *Proc. 156th Meeting of ISIJ and JIM: Joint Session on Current Advances in Materials and Processes*, The Japan Institute of Metals, Sendai, Japan, 2008, vol. 21 (2), p. 516.
- R.Z. Valiev, Y.V. Ivanisenko, E.F. Rauch, and B. Baudelet: *Acta Mater.*, 1996, vol. 44, pp. 4705–12.
- M.J. Zehetbauer, H.P. Stuwe, A. Vorhauer, E. Schafner, and J. Kohout: *Adv. Eng. Mater.*, 2003, vol. 5 (5), pp. 330–37.